João Machado Santos, Micael S. Couceiro, David Portugal, Rui P. Rocha
A Sensor Fusion Layer to Cope with Reduced Visibility in SLAM
Journal of Intelligent & Robotic Systems, JINT (2015).
DOI: 10.1007/s10846-015-0180-8

Noname manuscript No.
(will be inserted by the editor)

A Sensor Fusion Layer to Cope with Reduced Visibility in SLAM

João Machado Santos · Micael S. Couceiro · David Portugal · Rui P. Rocha

Received: 7th July 2014; Accepted: 15th November 2014

Abstract Mapping and navigating with mobile robots in scenarios with reduced visibility, *e.g.* due to smoke, dust, or fog, is still a big challenge nowadays. In spite of the tremendous advance on Simultaneous Localization and Mapping (SLAM) techniques for the past decade, most of current algorithms fail in those environments because they usually rely on optical sensors providing dense range data, *e.g.* laser range finders, stereo vision, LIDARs, RGB-D, *etc.*, whose measurement process is highly disturbed by particles of smoke, dust, or steam. This article addresses the problem of performing SLAM under reduced visibility conditions by proposing a sensor fusion layer which takes advantage from complementary characteristics between a laser range finder (LRF) and an array of sonars. This sensor fusion layer is ultimately used with a state-of-the-art SLAM technique to be resilient in scenarios where visibility cannot be assumed at all times. Special attention is given to mapping using commercial off-the-shelf (COTS) sensors, namely arrays of sonars which, being usually available in robotic platforms, raise technical issues that were investigated in the course of this work. Two sensor fusion methods, a heuristic method and a fuzzy logic-based method, are presented and discussed, corresponding to different stages of the research work conducted. The experimental validation of both methods with two different mobile robot platforms in smoky indoor scenarios showed that they provide a robust solution, using only COTS sensors, for adequately coping with reduced visibility in the SLAM process, thus decreasing significantly its impact in the mapping and localization results obtained.

Keywords SLAM · Reduced Visibility · Sensor Fusion · Robot Operating System (ROS)

1 Introduction

Over the past years, Simultaneous Localization and Mapping (SLAM) has been one of the most studied subjects in Robotics. It is a fundamental process which consists of building maps while, at the same time, estimating the robot position in the environment. SLAM is essential for autonomous mobile robots to accomplish useful tasks with no *a priori* information about the environment. There are many approaches to the SLAM problem [1] wherein each of them focuses on a particular issue. Despite all these approaches, namely focusing on large environments [2] or performing SLAM with multiple mobile robots [3], there are still many open challenges. For instance, when dealing with smoky, dusty, or foggy environments, commonly used range sensors for SLAM, like Laser Range Finders (LRFs), stereo vision rigs, or RGB-D sensors, are highly disturbed by noise induced in the measurement process by particles of smoke, dust, or steam which may obscure the environment.

J. Machado Santos
Lincoln Centre for Autonomous Systems
University of Lincoln, United Kingdom
E-mail: jsantos@lincoln.ac.uk

J. Machado Santos, M. S. Couceiro, D. Portugal, and R. P. Rocha
Institute of Systems and Robotics
University of Coimbra, Portugal
E-mail: {jsantos,micaelcouceiro,davidbsp,rprocha}@isr.uc.pt

Corresponding author: Rui P. Rocha
E-mail: rprocha@isr.uc.pt

This work is part of the CHOPIN[1] project which addresses search and rescue (SaR) missions in urban catastrophic scenarios (*e.g.* a fire in a large basement garage), by exploiting the human-robot symbiosis [4]. These scenarios are usually associated with environments with reduced visibility, which drastically decreases the progress of human rescuing forces and the accuracy and robustness of the robotic sensorial system, thus compromising the SLAM and overall navigation system. Due to the ever-increasing progress in the field of mobile robotics, it is foreseeable that in the short- and mid-term future, one will have mobile robots assisting and even replacing human operators in dangerous, dull or dirty tasks. This is the case of SaR missions which take place in extreme conditions and pose very difficult challenges, including navigating in reduced visibility conditions. The applicability of SLAM methods in these situations is scarce. Hereupon, it is necessary to propose techniques that can provide mapping and positioning information of robots within such harsh scenarios.

In this work, we address the problem of successfully performing SLAM in environments with reduced visibility conditions. Existing SLAM approaches require a "clean" environment, where the range sensor, which is usually based on light propagation, *e.g.*, LRF, stereo vision, time-of-flight (ToF) cameras, *etc.*, is not disturbed by particles of smoke, dust, or steam. The literature has shown that robots' perception can significantly benefit from merging sensing information from different sources. Therefore, in this article, we propose a multimodal sensor fusion layer, which encompasses information from sonars, a LRF, and an alcohol sensor, so as to overcome the lack of visibility and noise induced by smoke particles. The output of our system corresponds to a normalized confidence measure, evaluated for each sonar reading and corresponding section of the laser. We present and analyze both a preliminary heuristic based approach, and an adaptable fuzzy system to solve the multimodal sensor fusion problem. The system consists of a layer which uses the sensor data as input, and passes the processed sensor data on to the SLAM method. Our decision layer evaluates and generates the sensors readings and adapts them according to the visibility conditions. In other words, the proposed sensor fusion approach acts as a modular high level decision layer, regardless on the robotic platform and SLAM algorithm considered. In this work, we evaluate the sensor fusion layer using a Pioneer 3-DX and a Nomad Scout equipped with low cost sensors, such as a sonar ring, a LRF and a dust sensor, in order to perform SLAM in the aforementioned conditions.

The outline of the article is as follows: in the next section, related work on SLAM approaches evaluated under such harsh environments is reviewed. Then, a background study to assess the SLAM algorithm that best fits the goal of this work is presented. Afterwards, initial hardware tests are conducted and the main technical challenges involved in this work are discussed. Later, a preliminary version of an heuristic algorithm that explores the complementary characteristics of LRFs and sonars is described and validated through experiments in a room partially obscured by smoke. Afterwards, an improved fuzzy version of the aforementioned algorithm is presented and new experiments are conducted. In this work, two distinct mobile robots are used and their main technical issues are described. In the end, the output of the mapping task using our approach is compared to a common SLAM method that does not consider the smoke phenomenon. The results of both versions of the algorithm are discussed. Finally, the work ends with conclusions.

2 Related Work

Presently, all recognized algorithms for robot mapping have a common feature: they rely on probabilities. The advantage of applying probabilities is the robustness to measurement noise and the ability to formally represent uncertainty in the measurement and estimation process. Most of the probabilistic models used to solve the problem of mapping rely on Bayes rule [5]. These solutions account for sensor measurement noise and estimation uncertainty.

The literature is rich in SLAM methods. We can find methods that make use of Extended Kalman Filters (EKFs) [8][9] or even Rao-Blackwellized Particle Filters (RBPFs) [7][10]. Thus, the principle followed is similar: to incrementally compute joint posterior distributions over robot poses and landmarks. In addition, graph-based SLAM approaches [11] are also popular due the efficient way they deal with large-scale maps, and improvements in the sparse matrix calculations lead to a better graph optimization [12].

Most methods which are in focus nowadays have taken advantage of high scanning rates of modern Light Detection And Ranging (LIDAR) technology. These methods rely heavily on scan matching of consecutive sensor readings, with combination of other techniques, like multi-resolution occupancy grid

[1] `http://chopin.isr.uc.pt`

maps [13], or dynamic likelihood field models for measurement [14]. Despite the evident advances in research on SLAM, most approaches do not consider environments disturbed by smoke, dust, or steam.

In fact, when the scenario has reduced visibility, the majority of SLAM algorithms fail or present unsatisfactory results. The lack of visibility in the environment represents a challenge for SLAM algorithms, since it can partially or totally obscure the field of view that is used to map the scenario.

Brunner *et al.* [15] proposed a SLAM approach robust to smoke based on different sensing capabilities of visual cameras and thermal imaging cameras (TIC). The fundamental idea was to counterbalance the limitations of the visual camera in the presence of smoke with the robustness of a TIC in this situation. Experiments were performed in a smoky scenario using a robot equipped with a Raytheon thermal-eye 2000B infrared (IR) camera and a Point Grey Bumblebee XB3 camera set. Smoke was generated using a smoke machine. The authors concluded that a reasonable outcome can be obtained, but the localization accuracy decreased in the presence of smoke when only data from the TIC was used.

Deissler *et al.* [16] presented a SLAM algorithm based on a ultra-wideband (UWB) radar with a bat-type antenna array. This algorithm was developed for catastrophic scenarios, where the environment is corrupted with smoke or dust. Since it is a radar-based approach, the smoke/dust particles in the environment do not affect this algorithm. The biggest challenge is data association, *i.e.* assigning the time of flight of a given measurement from the radar to the corresponding landmark [16]. The authors solved this situation by using a RBPF for the data association process and an Extended Kalman Filter to estimate the state vector. The approach was tested through simulations and data acquired previously. The authors concluded that different propagation characteristics of walls, corners and other features in indoor environments can be used to distinguish those features, locate them, and use them as landmarks for navigation [16].

Castro *et al.* [17] proposed a reliable perception system based on sensor fusion between a millimeter-wave radar and a LRF. Although the LRF cannot penetrate heavy dust and smoke, the millimeter-wave radar can. The matching between LRF scans and radar scans was made by calculating the 3D Euclidian distance between each laser point and the closest radar target. The experiments were done using an all-terrain unmanned ground vehicle equipped with four LRFs and a frequency modulated continuous wave (FMCW) radar. The results obtained showed that most dust points in the LRF scans were removed. However, some dust points (false negatives) remained.

Although the work done by Sales *et al.* [18] does not involve SLAM directly, the vision system that is presented to determine the conditions of a given environment, *i.e.* to verify whether the environment is filled with smoke when detecting and tracking people, is relevant to the scope of this article. Three different person-following approaches were developed: sonar ring following, LRF following, and sonar time difference of arrival (TDoA) following. Sonar ring following is based only on ultrasound technology and its performance is the worst of the three approaches tested, as expected due to the low resolution of sonar sensors. However, in low visibility conditions, it is a better alternative than the LRF. The LRF following is based on scans from a LRF sensor to detect the person. Finally, the sonar TDoA following uses the radio and ultrasonic sensors to implement the person-following algorithm. This algorithm has achieved the best results in very different circumstances, even in smoky conditions.

Marti *et al.* [19] developed a localization method for smoky or dusty conditions. Their goal was to estimate the position of a mobile robot in front of points of interest (POI), such as doors or fire extinguishers. Their approach makes use of fingerprinting techniques and *ZigBee* beacons around the scenario to perform localization. Additionally, *ZigBee* beacons located in POI are equipped with a high luminosity Light-emitting diode (LED) panel. A visual positioning process is executed when approaching one of these panels. Since their location is known *a priori*, these panels can be used to determine accurately the robot's pose. This approach has been tested successfully in multiple scenarios, such as class rooms or corridors with stairs.

Pascoal *et al.* [20] carried out a set of tests in order to analyze the behavior of distinct LRFs within low visibility scenarios. Smoke was progressively injected in the scenario using a smoke machine and spread by means of a ventilator. The main conclusion obtained in their benchmarking experiments was that all the LRFs tested provide different levels of noisy and erroneous results with saturated outputs, which makes them almost unusable under these conditions. Similar conclusions were obtained by Tretyakov and Linder [21], and in a recent comparison presented in Pomerleau *et al.* [22], in which the LRF Hokuyo URG-04LX, also used in the results reported in section 5.4.1, presents the highest values of disparity and error in depth measurements, among of all compared LRFs.

As distinct to previously described works, we herein propose a multi-sensor approach based on a LRF and a sonar array which, despite being based on an affordable setup using only commercial off-the-shelf

(COTS) sensors, can provide a robust solution when LRF measures are partially disturbed by the presence of particles that reduce visibility.

3 Evaluation of SLAM algorithms in ROS

In this section, we introduce the Robot Operating System (ROS) framework used in this work and present the rationale behind the choice of the adopted grid map-based RBPF SLAM approach.

ROS[2] is a very popular robotics framework [27]. It provides several tools, libraries and drivers to enhance the development of new robotic projects. Also, it provides 2D and 3D simulation environments which increases its functionality. ROS has become one of the most used robotic frameworks, partly because of its characteristics, such as hardware abstraction and architecture. It enables researchers to quickly and easily perform experiments through the use of its integrated drivers, libraries, visualizers, message-passing and more. It is based on a graph intuitive architecture. All the processing takes place in *nodes* and data is exchanged using messages. The hardware abstraction layer in ROS, along with its messages service, allows the creation of new code that can be used in many different robotic platforms. Moreover, ROS provides a set of stable robotic software packages, like several SLAM algorithms, as shown in the course of this section.

Proprioceptive sensors are subject to cumulative errors when estimating the robot's motion. The high dimensionality of the environment, the problem of determining whether sensor measurements taken at different points in time correspond to the same object, and the fact that the world changes over time, represent the biggest challenges in SLAM [1]. Instead of developing a new SLAM approach from scratch, our work benefits from 2D laser-based SLAM algorithms available in ROS. However, a study of the current available algorithms was required in order to investigate which algorithm best fits our needs. Five 2D laser-based SLAM algorithms available in ROS were reviewed and evaluated, namely: *HectorSLAM* [13], *GMapping* [10], *CoreSLAM* [23], *LagoSLAM* [24] and *KartoSLAM* [25].

HectorSLAM[3] combines a 2D SLAM system based on robust scan matching and 3D navigation technique using an inertial sensing system [13]. The authors make use of the high update rate and the low distance measurement noise from modern LIDARs. The odometric information is not used, which gives the possibility to implement this approach in aerial robots, like a Quadrotor UAV, or in ground robots operating in uneven terrains.

GMapping[4] is a laser-based SLAM algorithm [10]. It has been proposed by Grisetti *et al.* [10] and is a RBPF SLAM approach. The authors compute an accurate particle distribution by taking into account not only the movement of the robotic platform, but also the most recent observations. In most particle filters, the proposed distribution uses the odometry motion model. However, when a mobile robot is equipped with a LRF, which is a very accurate sensor, the model of that sensor can be used, as it achieves extremely peaked likelihood functions. Based on this, the authors integrate the most recent sensor observation.

CoreSLAM[5] is a ROS wrapper for the original 200-lines-of-code tinySLAM algorithm, which is a laser-based approach created with the purpose of being simple and easy to understand with minimum loss of performance [23]. The algorithm is divided in two different steps: distance calculation and update of the map. In the first step, for each incoming scan, it calculates the distance based on a very simple PF algorithm.

The basis of graph-based SLAM algorithms is the minimization of a nonlinear non-convex cost function [24]. More precisely, at each iteration, a local convex approximation of the initial problem is solved in order to update the graph configuration. The process is repeated until a local minimum of the cost function is reached. However, this optimization process is highly dependent on an initial guess to converge. Carlone *et al.* [24] developed a new approach denoted as *LagoSLAM*[6] (Linear Approximation for Graph Optimization), in which the optimization process requires no initial guess. In addition, the technique can be used with any standard optimizer.

Another graph-based SLAM approach studied was *KartoSLAM*[7], which was extended for ROS by using a highly-optimized and non-iterative Cholesky matrix decomposition for sparse linear systems as its solver [25]. In this approach, each node represents a pose of the robot along its trajectory and a set of

[2] `http://www.ros.org/`
[3] `http://www.ros.org/wiki/hector_slam`
[4] `http://www.ros.org/wiki/gmapping`
[5] `http://www.ros.org/wiki/coreslam`
[6] `https://github.com/rrg-polito/rrg-polito-ros-pkg`
[7] `http://www.ros.org/wiki/karto`

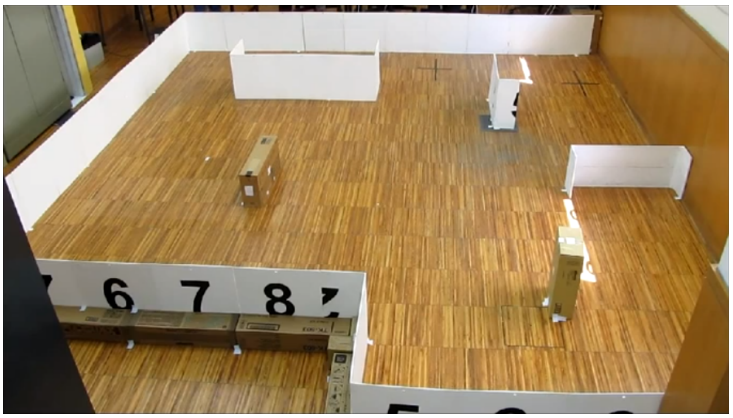

Fig. 1: The test arena (*MRL arena*).

Table 1: Error estimation for each algorithm in a test arena (simulation and real world experiments). All units in pixels.

Simulation Experiments				
HectorSLAM	Gmapping	KartoSLAM	CoreSLAM	LagoSLAM
0.4563	0.4200	0.5509	11.8393	1.4646
Real World Experiments				
HectorSLAM	Gmapping	KartoSLAM	CoreSLAM	LagoSLAM
1.1972	2.1716	1.0318	14.75333	3.0264
0.5094	0.6945	0.3742	7.9463	0.8181
1.0656	1.6354	0.9080	7.5824	2.5236

sensor measurements. These are connected by arcs which represent the motion between successive poses. For each new node, the map is computed by finding the spatial configuration of the nodes which are consistent with constraints from the arcs.

All five SLAM techniques described above were tested in ROS using 2D simulations and real world experiments. Simulations were performed in Stage[8], a realistic 2D robot simulator integrated in the ROS framework. Additionally, tests were also conducted with a physical robot in a real world scenario, displaying the behavior of these SLAM packages in real world situations and in the absence of perfect simulated conditions. Despite having perfect conditions in Stage simulations, like noise free odometric and range sensing information, there are some imperfections in the final result, which may be due to other phenomena, such as linearizations or the particle filtering step in Monte Carlo approaches. Although, noise could be introduced in Stage for both odometric and sensor readings, the behavior of all aforementioned methods in noise free scenarios can provide more information about the difference in performance between noise free environments and noisy environments, allowing to check how each method will deal with small concentrations of smoke. In all experiments, ROS was used and the robot was teleoperated. Note also that the abstraction layer provided by ROS allows to use the same code for both simulation and real experiments. Note that the update rate of the Hokuyo URG-04LX-UG01 LRF used in the experiments is only 10 Hz and Stage uses a similar maximum update rate. In order to deal with this, the robot was driven with low angular and linear speeds. In the tests that were conducted, the output of each approach described previously was the respective generated 2D occupancy grid map.

To evaluate the quality of the maps obtained in the experiments performed, an analysis of the error between the generated map and the ground truth was conducted. The test arena on Fig. 1 was adopted, and a performance metric based on the k-nearest neighbor concept was used. In order to adopt this metric, the best fit alignment between the ground truth and the map obtained was computed using intensity-based image registration tools. In [26], the metric is described in detail and more results are presented. The numeric results are shown in Table 1.

From the analysis of the results, it was observed that *GMapping* and *HectorSLAM* generated the map with the lowest error. On the other hand, *KartoSLAM* presented a slightly greater error, while results

[8] `http://www.ros.org/wiki/stage`

Table 2: CPU usage (%) of the 2D SLAM approaches: mean ($\bar{x}$), median ($\tilde{x}$) and standard deviation (σ) values.

	HectorSLAM	Gmapping	KartoSLAM	CoreSLAM	LagoSLAM
$\bar{x}$	6.1107	7.0873	5.4077	5.5213	21.0839
$\tilde{x}$	5.9250	5.5800	5.3000	5.4400	21.2250
σ	1.993	4.4287	1.3018	1.6311	2.1684

of *CoreSLAM* presented the highest error value. *GMapping* is an extremely optimized PF algorithm with an improved resampling process, and this justifies the quality of the resulting map. Also, the scan matching process of *HectorSLAM* showed its efficiency. Nevertheless, it must be noted that the low speed commands given to the robot, in order to compensate the rate update from the LRF, have some influence in the results. Both *KartoSLAM* and *LagoSLAM* mapped successfully the arena. However, *LagoSLAM* obtained the greatest error (excluding *CoreSLAM*). In real world experiments, the error increased for all approaches as expected due to noisy input. In the case of *KartoSLAM* algorithm, the error obtained in the real world experiments was not much higher than the error in simulations. The lower results of *CoreSLAM* in all experiments showed that its loop closure procedure rarely converges.

Beyond the error analysis conducted, an evaluation of the computational load using each technique was carried out (see Table 2 for more details). All tests were conducted in a laptop equipped with and Intel Core i7-3630QM and 8 Gb of RAM. *LagoSLAM* presented the highest percentages of central processing unit (CPU) usage. Moreover, the values obtained are quite distant from the other four algorithms. The resources needed by the other four approaches during the experiments were similar and remained low. This analysis revealed that all five algorithms are quite efficient in terms of resources required and can be adopted for on-the-fly SLAM, in field experiments to map generic 2D scenarios.

Both *GMapping*, *HectorSLAM* and *KartoSLAM* are strong candidates for our work. However, *HectorSLAM* relies only on scan matching and it does not make use of odometry, which is a disadvantage in reduced visibility condition, wherein typical range sensors fail and the odometry has a fundamental role of estimating the robot pose. On the other hand, both *GMapping* and *KartoSLAM* showed its robustness in every test and the error and CPU load always remained low. It is noteworthy that goal of this work is to provide a decision layer for low visibility conditions that is decoupled from the SLAM algorithm. The present comparison gives us an idea of which algorithm can be used to achieve the best results with our layer. Both methods, *GMapping* and *KartoSLAM*, present very solid results. However, *GMapping* is one of the most widely used SLAM methods, and has proven its use in more complex and demanding scenarios. Also, this method has been adapted for every new version of ROS and has a better support in the ROS community. So, the logical choice is to use *GMapping* as the base algorithm for this work, which combines both scan matching and odometry in order to minimize the number of particles and improve the accuracy of the estimated pose. More details about the SLAM evaluation conducted can be found in [26].

4 Sensor limitations and technical challenges

The implementation of a SLAM technique highly depends on the correct choice of sensors, which is related with the environment where the robot operates. The accuracy and reliability of common optical range sensors, *e.g.* LRF or stereo-vision sensors, drastically decreases under low visibility conditions. As mentioned before, LRFs are one the most adopted range sensors in SLAM. They are extremely accurate in "clean" environments and easy to use. However, the main goal in this work is to develop and verify a SLAM approach in environments with smoke, dust, or steam particles, which easily corrupt LRF readings. In order to decrease the impact of such disturbances in SLAM algorithms using optical sensors, multimodal sensor fusion is required, by merging information provided by different types of range sensors. An optical-based range sensor (LRF, stereo camera, *etc.*), which is very effective in normal visibility conditions, can be combined with another sensor that is less disturbed, or even immune, to visibility disturbances. Such auxiliary sensor may provide sparser and less accurate range measurements, which may still be the only valid readings in low visibility conditions. Possible combinations include LRF with sonars, LRF with ToF cameras and sonars, LRF with UWB radars, *etc.* Sonars are the immediate economic and widely available choice, as they use the propagation model of acoustic waves at higher frequency than the normal range

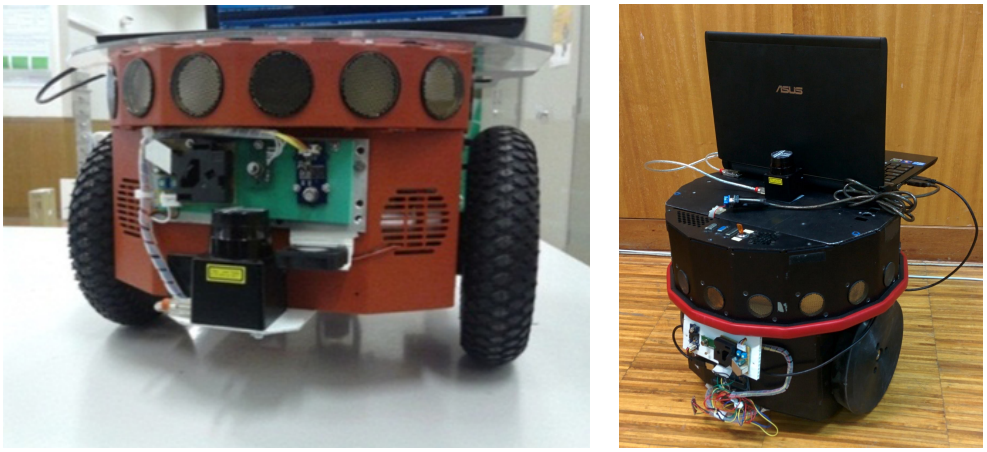

(a) The Pioneer 3-DX. (b) The Nomad Scout.

Fig. 2: Robotic platforms used in this work.

of human hearing to extract information of the surroundings. Since they use acoustic waves, they are immune to smoke or dust particles.

In this work, two differential mobile robotic platforms were used: the Pioneer 3-DX and the Nomad Scout (see Fig. 2). The Pioneer 3-DX is equipped with an array of 8 sonars, being a very versatile and robust mobile robot. It is a two-wheels differential robotic platform commonly used for research worldwide. Its frontal sonar ring comprises 8 SensComp's Series 600 Instrument grade Electrostatic Transducer[9] disposed at angles: -90^o, -50^o, -30^o, -10^o, 10^o, 30^o, 50^o and 90^o. Each ultrasonic sensor has a beam angle of 15^o at $-6dB$. Its maximum range is about 5 meters and the field of view (FoV) of the sonar ring is about 196^o. While the Pioneer robot has a 8 sonar array, the Nomad has an array of 16 uniformly distributed sonars with an overall FoV of 360^o. Also, the characteristics of the sonars used in each platform are different. The Scout robot uses a Polaroid 6500 range board with a FoV of about 20° degrees. The performance of both arrays will be discussed in the following sections.

The LRF available for the experiments reported herein was an Hokuyo URG-04LX. It has a maximum range of 5.6 meters, an angular resolution of about 0.36^o, and a FoV of 240^o. In order to guarantee a common area with the range data information from the LRF and the sonar arrays, the information of some of the sonars were discarded. More specifically, while for the Pioneer 3-DX all 8 sonars can match the LRF readings, in the Nomad Scout only 9 sonars were considered (see sonars in Fig. 2b). The sonars arrangement in both robots is illustrated in Fig 3.

Before proceeding to the development of the proposed multi-sensor fusion methods to perform SLAM under reduced visibility conditions, the behavior of each ranging sensor was evaluated in several situations.

In a first trial, the Pioneer 3-DX equipped with the Hokuyo LRF was placed in front of a flat wall and smoke was injected between the robot and the wall. The smoke machine used was a Magnum 800[10]. Fig. 4 shows an example of the LRF readings before (Fig. 4a) and after (Fig. 4b) the injection of smoke. As expected, even in small concentrations, smoke highly affects the sensor readings.

In order to successfully perform a mapping task under these conditions, sonars can be useful to compensate the misreadings of the LRF due to their immunity to smoke particles. Regarding the sonar ring of the Pioneer 3-DX, a somehow unexpected behavior occurred in some situations, which made the development of the algorithm much more challenging. Consider a long corridor as shown in Fig. 5a, where the robot is positioned in the middle of an obstacle-free corridor. The only sonars in the P3-DX capable of detecting walls are the ones positioned at -90^o and 90^o. Due to the small FoV of each sensor, approximately 15^o, obstacles are only detected when the incident beam is normal or nearly normal to them (*cf.*, Fig. 5b). Hereupon, it is necessary to discard these erroneous values, corresponding to saturated values, *i.e.*, the maximum range of the sonar. This is a necessary preprocess step, not only because the saturated values do not allow to evaluate the "quality" of the LRF readings, but also do not allow to map the environment in severe visibility conditions, where the LRF readings are all wrong.

Following the previous experiment, the Scout robot was tested in the same conditions, *i.e.*, it was deployed in the same corridor as the Pioneer 3-DX. The result is shown in Fig. 6. Each cone represents

[9] `http://www.senscomp.com/pdfs/series-600-instrument-grade-sensor.pdf`

[10] `http://www.martin.com/product/product.asp?product=technofog&newseg=ent&mainseg=ent`

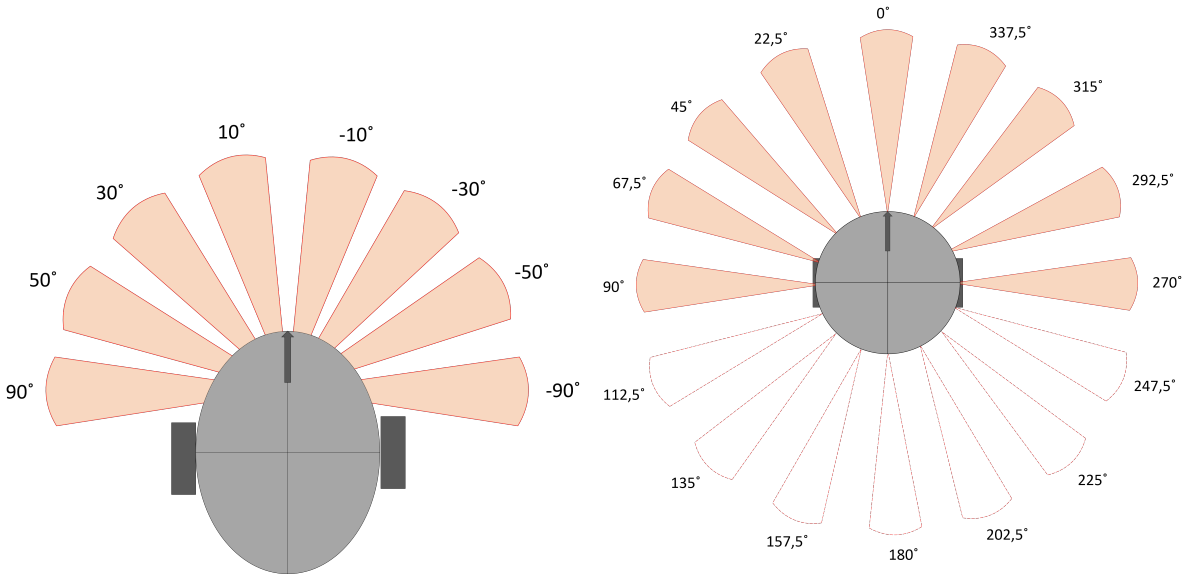

(a) The Pioneer 3-DX. (b) The Nomad Scout.

Fig. 3: Sonars displacement in both robots used in this work.

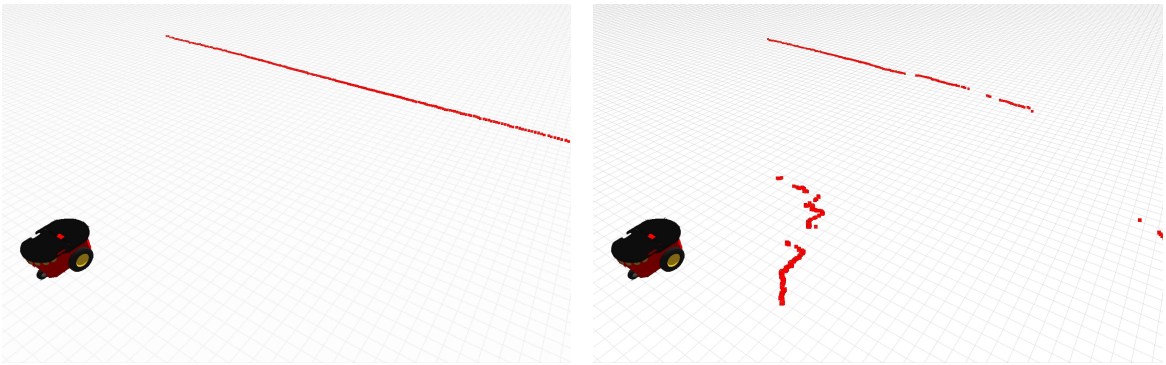

(a) LRF readings without smoke. (b) LRF readings with smoke.

Fig. 4: Performance test of the LRF against a wall, with and without smoke.

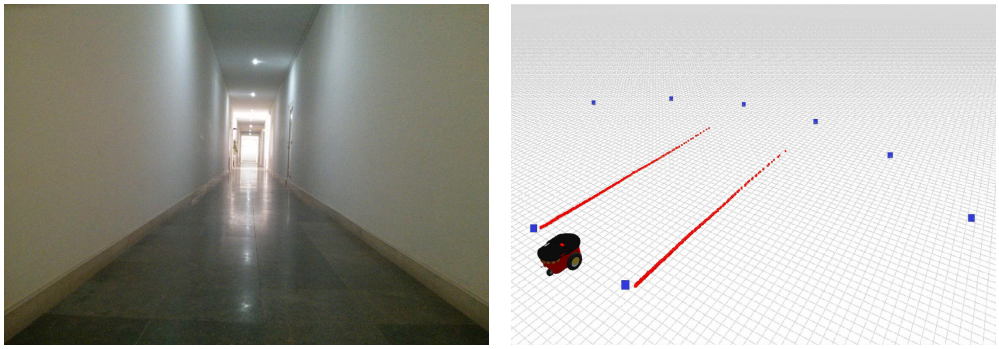

(a) Corridor. (b) Sonar readings of the Pioneer 3-DX.

Fig. 5: Behavior of the Pionner's sonar ring in a plain corridor. Red dots are the LRF readings and blue dots are the sonars readings.

the sonar reading, where the size of the cone depends in the distance measured. As it can be noted, the side sonars are able to detect the walls even when the incident sonar beam is not normal to the wall

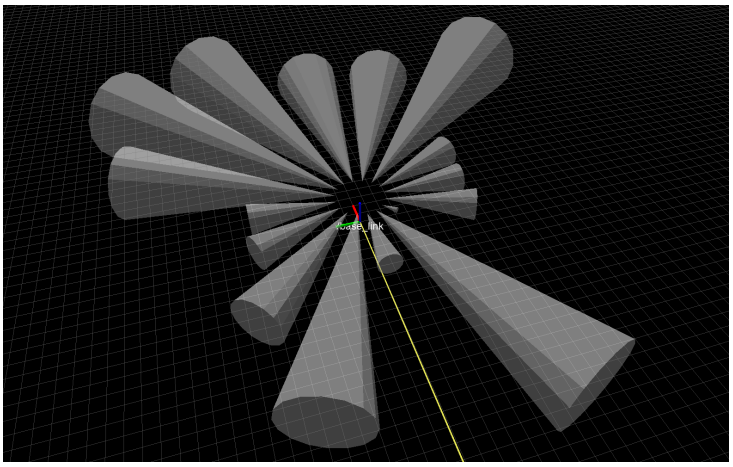

Fig. 6: Sonar readings of the Nomad Scout in the same plain corridor.

surface, providing more reliable data than the Pioneer. The output from Scout's sonar ring is more stable and it behaves closer to expected, although still providing a small subset of saturated readings. During the development of the sensor fusion approach for reduced visibility scenarios described in this article, the Pioneer 3-DX was replaced by the Nomad Scout platform due to the more stable behavior provided by its sonar ring. This was important to improve our method and results.

In these preliminary tests, it was verified that the information obtained using only two types of sensors would be insufficient under certain situations. This is the case, for example, when the comparison between both is not possible (*i.e*, saturated sonar readings and noisy laser scans). When the smoke density is very high, from the LRF standpoint, it forms an almost indistinguishable obstacle. Other challenging situations occurs when the robot rotates and the sonar saturates due to their low resolution, which is extremely problematic. Therefore, an additional sensor to inform about the concentration of smoke in the environment was required. Typically, we would use a dust sensor in this context. However, as the smoke machine available for our experiments produces a glycol-based vapor, an alcohol sensor was used instead. This technological choice allowed to detect different concentrations of glycol-based vapor, thus emulating a dust sensor in our experiments. The sensor model used was the MQ303A[11], manufactured by Seeed Studio, in which the output voltage is inversely proportional to the alcohol concentration in the air.

5 Multimodal Sensor Fusion Method for Low Visibility Scenarios

5.1 Mapping with sonars

The worst-case situation for the SLAM algorithm is when the smoke concentration is so high that the whole LRF readings are corrupted. In such extreme case, the mapping task must be done using only the sonar ring. Hence, it is important to verify whether *GMapping* is able to successfully map the environment using only sonars data. However, this work is not intended to be limited to the use of the *GMapping* SLAM approach only. Therefore, we developed an "intelligent" layer which fuses the output of each sensor and adjusts, rectifies, or ignores certain information according to the situation. A ROS node was developed to convert the data received from the sonar ring to laser scan data. Algorithm 1 presents a high-level code of the implemented conversion of sonar readings (represented as a point cloud message) to a laser scan message.

Several runs in a small scenario, denoted as *MRL arena* (see Figures 1 and 7a), were conducted in order to refine the parameters of *GMapping* so that it provides the best possible map using only sonar data. Yet, the quality of the resulting map is expected to be low, due to the low resolution of sonars. Moreover, the sonars return the maximum range (5.0 meters) when they do not receive the sound wave echo, *i.e.* when they are unable to detect any obstacle within their range. Consequently, in order to decrease the aforementioned issue related with the non-normal surfaces, the range of each sonar has been limited to a maximum of 2.5 meters, thus avoiding misreadings from the robot while rotating.

The impact of the number of particles, map resolution, and temporal thresholds has been tested too. After a fine tuning of these parameters by trial-and-error using empirical data, the best results were

[11] `http://www.seeedstudio.com/depot/images/product/MQ303A.pdf`

Algorithm 1: PointCloud message to LaserScan message (conversion of sonar readings).

input : sensor::msgs::PointCloud input_pcl
output: sensor::msgs::LaserScan sonar_scan

transformPointCloud(input_pcl,pcl_transformed,target_frame); //transforms sonar points from the local sonar frame to the Laser reference frame
range_min_sq = range_min × range_min;
ranges_size = ceil($\frac{angle\_max - angle\_min}{angle\_increment}$);
ranges[ranges_size] = range_max + 1.0;
for *each point in pcl_transformed* **do**
  if *x!=0* **and** *y!=0* **then**
    range_sq = x×x + y×y;
    if *range_sq* <*range_min_sq* **then**
      continue;
    end
    angle=atan2(x,y);
    for $j = \forall\ \theta \in [-\frac{angle}{2}, \frac{angle}{2}]$ **do**
      if *j* <*angle_min* **or** *j* >*angle_max* **then**
        continue;
      end
      index = $\frac{j - angle\_min}{angle\_increment}$;
      if *range_max* =>*range_sq* **then**
        sonar_scans.ranges[index] = $\sqrt{range\_sq}$;
      end
    end
  end
end
publish(sonar_scan);

Table 3: Parameters used in *GMapping* algorithm to successfully map the *MRL arena* using only sonar data.

Parameter	Value	Parameter	Value
maxUrange	16.0	sigma	0.05
kernelSize	1	iterations	5
linearUpdate	0.5	angularUpdate	0.8
temporalUpdate	3.0	resampleThreshold	0.5
particles	30	delta	0.01

achieved with the values presented in Table 3. Several other parameters were tested, such as the number of iterations of the scan matching and the angular resolution.For instance, in Fig. 7, the maps obtained with angular resolutions in different trials are shown.

The angular resolution of 0.0175^o has been chosen, since it achieved a relatively accurate map and represents the same value of angular resolution as the LRF used in our experiments.

5.2 Overview of the proposed multimodal sensor fusion laser

The proposed architecture receives messages from both range sensors and treats the data taking into account the time stamps coming from both scans. The need to synchronize messages and to minimize the delay in the processing time dictates that any of the algorithms has to be simple and effective. Message synchronization between the sonar ring and the LRF is possible due to the message filter API[12] available in ROS. Whenever a *LaserScan* or a sonar *PointCloud* message arrives, their time stamps are compared using an approximate time policy. After that, the point cloud received is transformed from the sonar frame to the LRF frame, in order to analyze and compare both readings in the same reference frame. Each point in the point cloud, corresponds to a section of the sonar simulated "scan". The section is determined by transforming the point to the polar form and using the FoV of the sonar.

[12] `http://wiki.ros.org/message_filters`

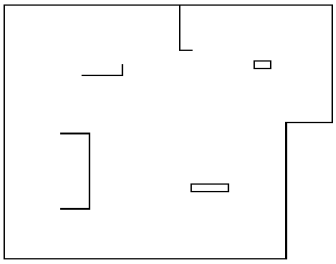

(a) *MRL arena* (4.57×4.04m).

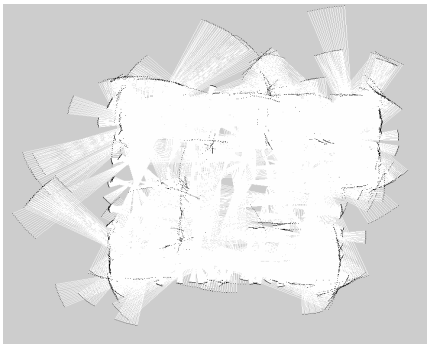

(b) Angular resolution of 0.01^o.

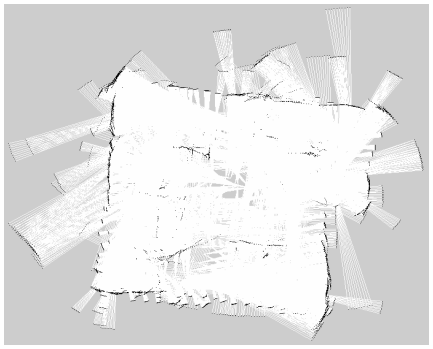

(c) Angular resolution of 0.0175^o (the same resolution of the Hokuyo).

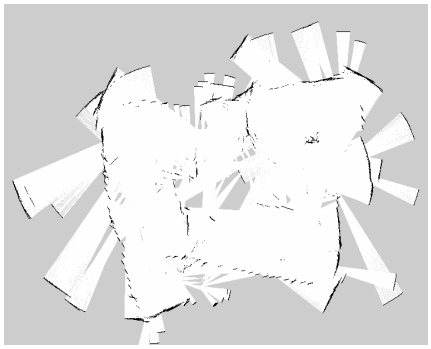

(d) Angular resolution of 0.0044^o.

Fig. 7: Resulting maps of some of the experiments conducted with *GMapping* fed by sonars in the *MRL arena* depicted in Fig. 1, page 5.

An overview of the aforementioned process is presented in Fig. 8. Two algorithms were developed in the course of our work, corresponding to different stages of the research study. They are presented in the following subsections. These algorithms fit into the "SmokeNav" box in Fig. 8. The layer in this box adapts to any set of range data and provides the filtered data to potentially use any generic LRF-based SLAM algorithm under low visibility conditions, in the form of a combined *LaserScan* ROS message. In this way, although we have chosen *GMapping* to perform the SLAM task, the software module related with the SLAM technique being used is interchangeable and any SLAM technique can be used with the *SmokeNav* layer we developed.

The information arriving from the alcohol sensor is constantly monitored to infer the visibility conditions of the environment. It should be noted that the data of each sensor is published at a rate of about 10Hz.

5.3 *SmokeNav v1*: Heuristic Model

In a preliminary attempt to propose a SLAM system that would perform well in smoky environments, a deterministic method for our sensor fusion layer was developed. This approach considers a set of heuristics supported by the conclusions obtained in preliminary tests.

For each sonar section τ_i (*cf* Fig. 9), the corresponding section in the LRF laser scan message is evaluated. With that purpose, a threshold MAX_DIFF is calculated as follows:

$$\overline{r} = \frac{1}{N_s} \sum_{i=1}^{N_s} r_i, \tag{1}$$

$$MAX\_DIFF = \alpha_{step} \cdot \overline{r}, \tag{2}$$

where $\overline{r}$ is the mean value of all ranges of the LRF in the given section τ_i , N_s is the number of LRF readings for the section τ_i and α_{step} is the laser scan angle increment (in rad). Afterwards, the squared

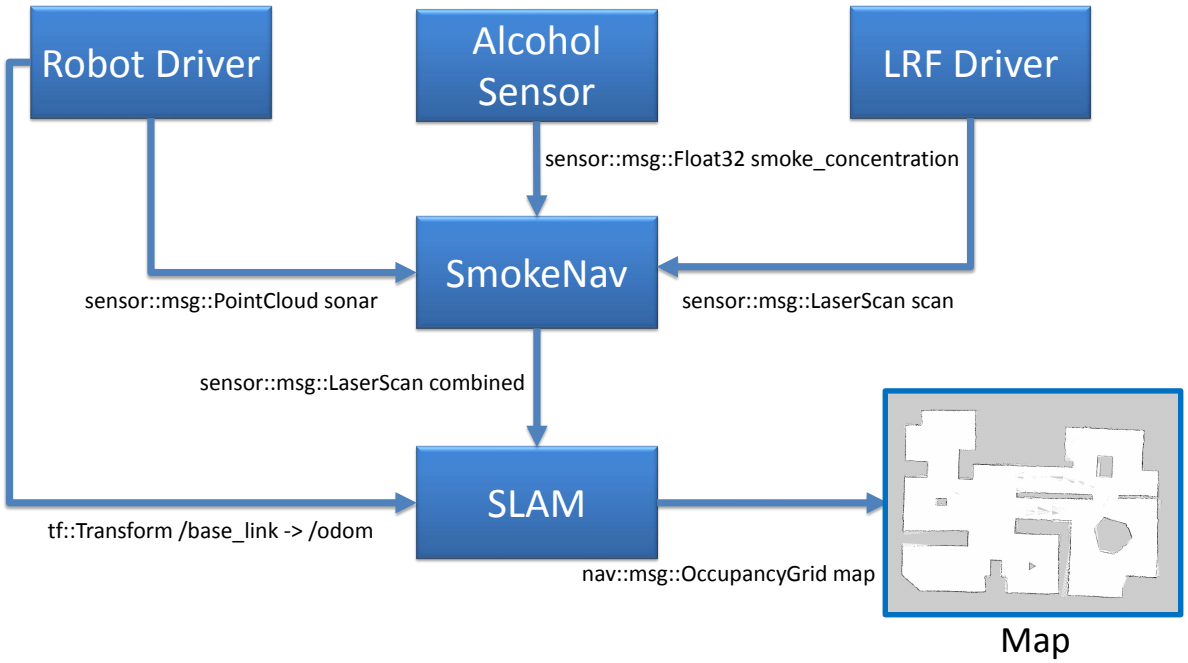

Fig. 8: Overview of the *SmokeNav* layer integration.

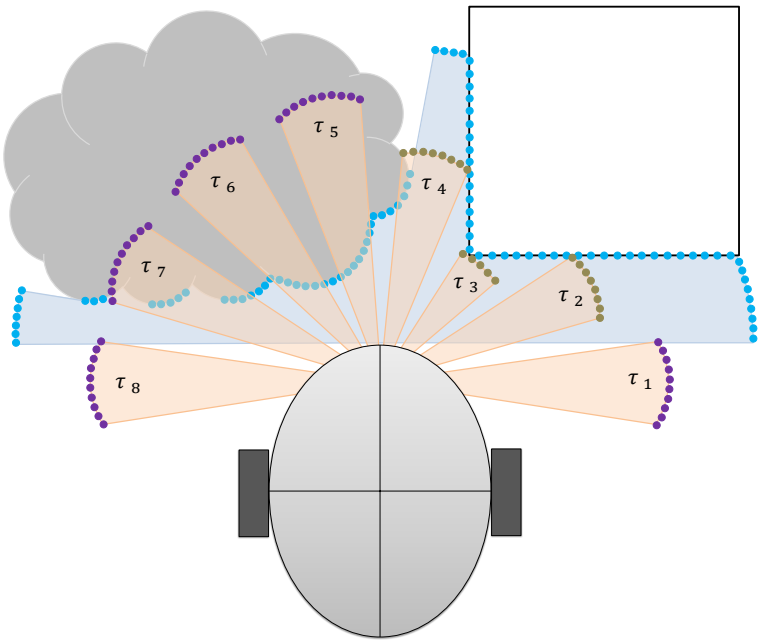

Fig. 9: Pioneer 3-DX sensors arrangement: LRF (blue dots) vs sonar array (purple dots). Each section is labeled with τ.

differences of the ranges of all readings in a given section τ_i are determined and, if any of the absolute values of these differences is greater than MAX_DIFF, a zero-crossing[13] mechanism is applied. The mechanism basically consists of: if one third of the differences (*i.e.*, $\frac{(N_s-1)}{3}$) lead to sign changes, the laser section will be discarded or replaced by the respective sonar reading, if it is valid.

As mentioned before, using only the range sensors is not enough to detect smoke and the information provided by the alcohol sensor needs to be integrated. The alcohol sensor detects the artificial smoke relatively fast, but it is slow to recover when the smoke concentration is decreasing. To overcome this issue, two stages are identified: increasing and decreasing smoke concentration. According to these stages, smoke

[13] A "zero-crossing" is a point where the sign of a function changes (*e.g.* from positive to negative).

thresholds will vary. If the value of sonar readings do not match measurements taken by laser scans, and the smoke levels detected by the alcohol sensor hits values below a minimum threshold $SMOKE\_MIN$ $(130mV)$[14], a greater confidence is given to LRF readings. If the alcohol sensor retrieves values greater than $SMOKE\_MIN$, sonar readings are superimposed to LRF readings. In this situation, when high differences between the laser and sonar readings in the same section τ_i occur, only the sonar ring data from is used, as explained before.

If the smoke density surpasses the maximum smoke threshold, the mapping task will be performed solely with the sonar data. However, due to the slow decreasing curve of the alcohol sensor, this threshold was decomposed in $SMOKE\_MAX\_UP$ $(200mV)$ and $SMOKE\_MAX\_DOWN$ $(240mV)$, for the case where the smoke is increasing or decreasing, respectively. Algorithm 2 presents this set of rules.

After the evaluation of every sonar section, all the gathered information is used to build the combined *LaserScan* ROS message. When smoke is detected in a given section τ_i , the measurement of the LRF is corrected if the sonar is available, or ignored if the sonar is unavailable. The sections of the LRF scan not covered by the sonars (due to its reduced FoV) will be filtered according to the state of the adjacent sections. Basically, these sections that only possess laser data are accepted only if adjacent sections are not considered as being corrupted with smoke.

Algorithm 2: *SmokeNav v1*: Deterministic Model Pseudocode

```
1  if smoke concentration < SMOKE_MIN then
2      only LRF is used;
3  else
4      for each sonar section do
5          if smoke increasing then
6              if smoke concentration < SMOKE_MAX_UP then
7                  Sonar is superimposed to LRF
8              else
9                  only Sonar is used
10             end
11         else
12             if smoke concentration < SMOKE_MAX_DOWN then
13                 LRF is superimposed to Sonar
14             else
15                 only Sonar is used
16             end
17         end
18     end
19 end
```

5.3.1 Results and Discussion

In order to validate this preliminary heuristic algorithm, several real world experiments were performed with the available Pioneer 3-DX robot in a smoky scenario. A large arena was built in a class room of the Department of Electrical and Computer Engineering of the University of Coimbra. The resulting arena, denoted as *R3.2 arena*, is shown in Fig. 10a. Additionally, a ground truth map of the arena was built (Fig. 10b). Also, *GMapping* was first evaluated in this arena with clean conditions. The resulting map is shown in Fig. 10c.

In order to extract relevant data and validate the algorithm, several runs using the Pioneer 3-DX robot were performed in the *R3.2 arena* under different visibility conditions. All robot's sensor data (LRF, sonars, odometry, and alcohol sensor) was recorded using the the *rosbag* tool available in ROS. This allowed running the algorithm after the experiment, and also testing *GMapping* in the same exact conditions without the *SmokeNav* layer, and verify if there were significant improvements, *i.e.* if the algorithm was able to successfully map in the presence of smoke.

The robot started in a clean zone in every trial. Afterwards, the robot started moving, and smoke was injected at different intensities in an opposite area. In these experiments, the robot was teleoperated using a Wiimote. Results of three trials under different conditions of smoke are shown in Fig. 11.

As one may observe, in all trials when *GMapping* is fed solely with laser data, *i.e.*, without the *SmokeNav v1* layer, it is unable to map zones corrupted with smoke. Even when the robot leaves the smoky zone, the estimation of the robot's pose becomes erroneous and the algorithm is not able to

[14] As mentioned before, note that our alcohol sensor provides an output voltage that is inversely proportional to the alcohol (simulated smoke) concentration in the air.

(a) Photo of the arena.

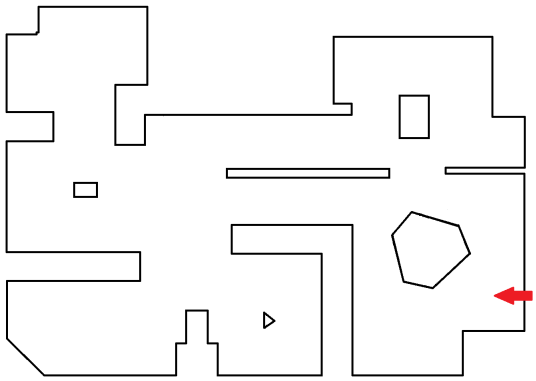

(b) Ground truth map.

(c) Photo of the smoky conditions in the arena.

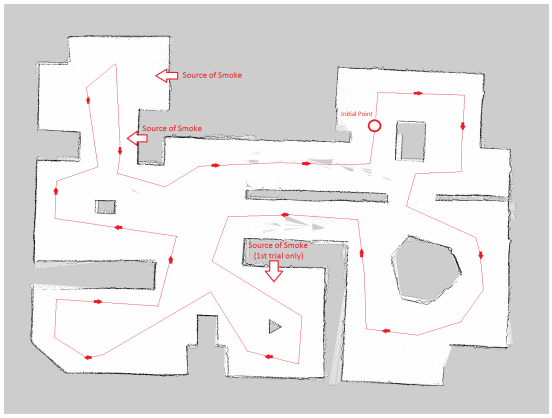

(d) Resulting map of a run with *Gmapping*.

Fig. 10: The *R3.2 arena* with dimensions: 13.63 × 9.87 meters. The arrow in Fig. 10b represents the viewpoint of Fig. 10a

correctly recover and update the pose. This is expected since the algorithm is only using the LRF and the scan matching process fails due to the false readings.

From the analysis of the results, it can be seen that the first sensor fusion algorithm proposed was able to map the arena even when the smoke density was high. However, when the switching from the LRF to sonars occurred, the quality of the map drastically decreased, as expected. This happened not only because of the low resolution of the sonars, but also due to their previously mentioned misbehavior. This is verified in Figures 11a and 11b, where the robot crossed regions with a higher density of smoke, moments after the beginning of the mapping task. In the remaining trials, the smoke was injected only in the latest region to be mapped. For this reason, *GMapping* using only LRF data did not perform as poorly as one could expect. Nevertheless, in the second and third trials, the impact of smoke in the mapping task is visible: the upper left corner was not correctly mapped. Due to the high smoke density, the scans returned by the LRF resemble a dense obstacle in that area. However, when *GMapping* was fed with sonar data, that zone was eventually mapped, though the quality of the mapping was low.

From the analysis of the results, it was concluded that this preliminary approach has several weaknesses and is not robust enough for harsh conditions. The behavior of the sonar ring is erroneous and not stable enough. Most of the times, the SLAM algorithm is relying only on the readings provided by the sonars, which does not provide enough data for localization. Also, the quality of the obtained maps is low. In the next section, we present a novel multi-sensor fusion approach based on fuzzy logic aiming to overcome some of these issues.

5.4 *SmokeNav v2*: Fuzzified Model

The method presented in the previous subsection revealed that it is possible to map an environment under low visibility conditions using only commercial off-the-shelf sensors. However, the obtained results were

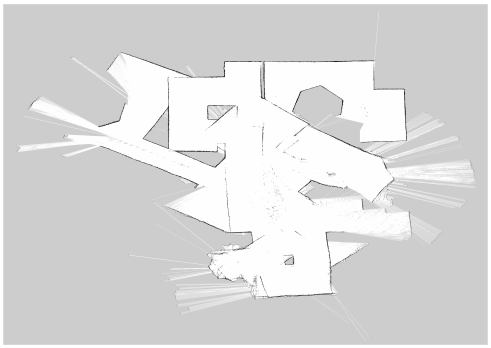

(a) Trial 1: *GMapping* only with LRF data.

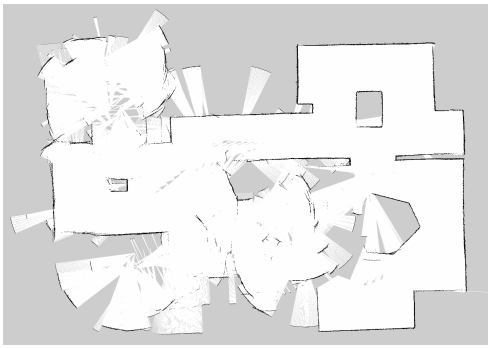

(b) Trial 1: *GMapping* with the *SmokeNav v1* layer.

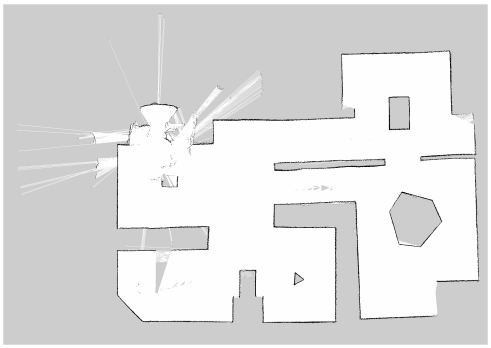

(c) Trial 2: *GMapping* only with LRF data.

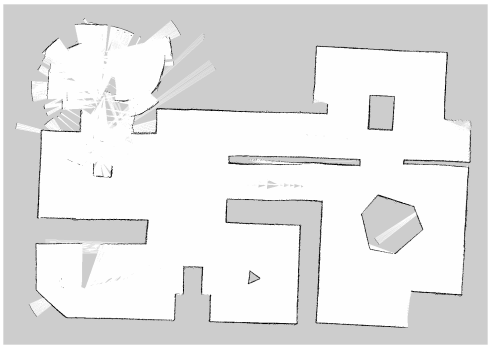

(d) Trial 2: *GMapping* with the *SmokeNav v1* layer.

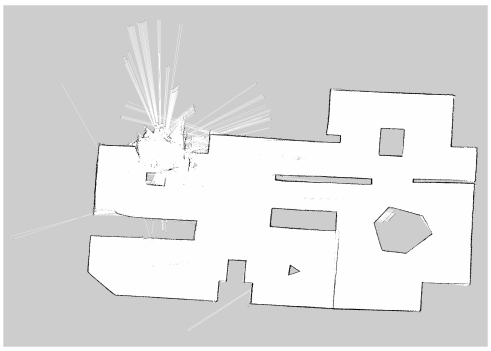

(e) Trial 3: *GMapping* only with LRF data.

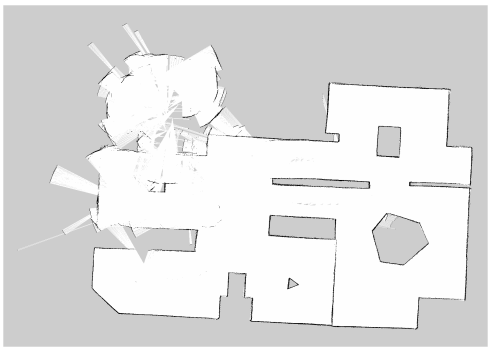

(f) Trial 3: *GMapping* with the *SmokeNav v1* layer.

Fig. 11: Results of three trials. Left images are the resulting maps from *GMapping* only with LRF data and the right images are the maps obtained using the preliminary multimodal sensor fusion technique.

bellow expectations and far from being applicable under real world situations. The need to improve the method arose and this section presents a newer, more robust, and more elaborated version. Additionally, we chose to use the Nomad Scout robot, which was available at this stage of the work, taking advantage of its more reliable sonar ring, as it was discussed in sec. 4.

In order to overcome the limitations of the deterministic approach described in the previous section, we developed an adaptive fuzzy logic system to handle the sensing information arising from the sonars, LRF, and alcohol sensor, by following a similar approach to our previous work in another domain [29]. This was the base for the development of the *SmokeNav v2* layer. Other proposals with different formalism to multimodal sensor fusion, such as Bayesian decision analysis [30], could be adopted as well. The successful development of a fuzzy model is a complex multi-step process, in which the designer is faced with a large number of alternative implementation strategies and attributes [31].

In sum, based on the information extracted from the inputs, namely the alcohol sensor, sonar and LRF readings, the fuzzy logic system can infer normalized confidence measures, which can be used to

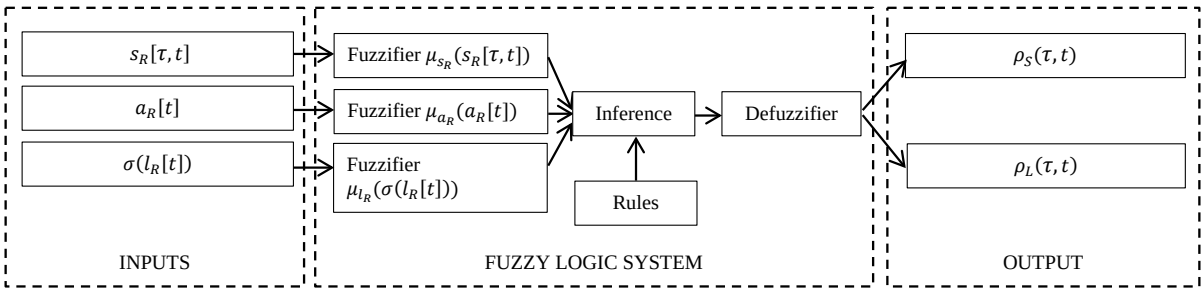

Fig. 12: Fuzzy logic system to choose the adequate reading.

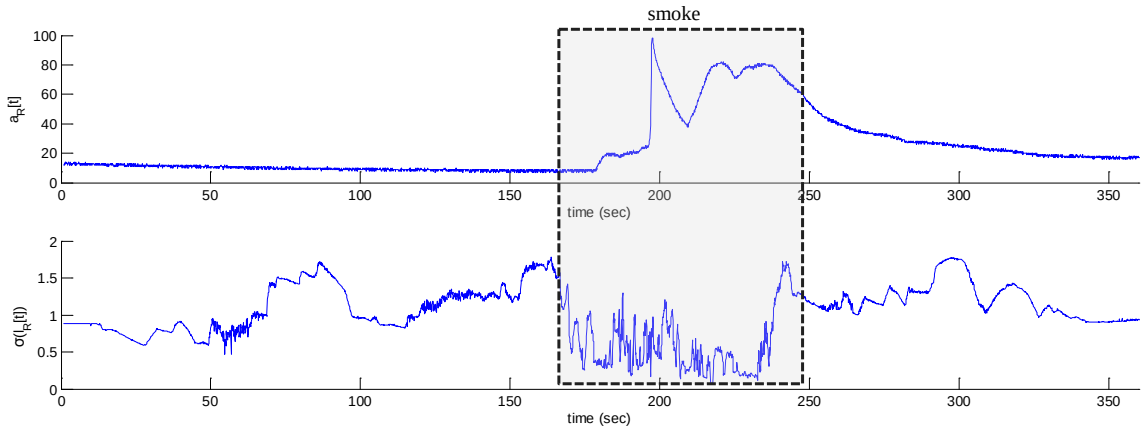

Fig. 13: Sensor readings over time: on the top, alcohol sensor readings, $a_R[t]$, over time; on the bottom, standard deviation, $\sigma(l_R[t])$, of the LRF readings over time. The alcohol sensor presents significant variations when facing smoke. However, it also presents a slow response. On the other hand, the standard deviation of the laser readings proves to be a relevant complement to the decision-making.

decide on whether to choose the sonars or the LRF data (Fig. 12). These two outputs can be perceived as the confidence on a given sonar reading (ρ_S) or the probability on trusting on the laser readings within the same section τ_i of that sonar (ρ_L). It is noteworthy that these probability measures are not mutually exclusive. In other words, it is possible to reject the readings provided by both sources, *e.g.* a high intensity of smoke detected by the alcohol sensor and a sonar reading above 2.5 meters is likely to result in probabilities on trusting in both sources near to zero. In these cases, *GMapping* will be fed with a value greater than the maximum range of the sensor, thus considering it as a saturated reading.

The control architecture presented in Fig. 12 is executed at each iteration t, and for each section τ (Fig. 9), thus returning the probability of accepting the sonar τ at time t, $\rho_S(\tau,t)$, and the probability of accepting the LRF readings from the same section at time t, $\rho_L(\tau,t)$. The inputs of the fuzzy system comprise the sonar reading from section τ, $s_R[\tau,t]$, the alcohol sensor reading, $a_R[t]$, and the standard deviation of LRF readings, $\sigma(l_R[t])$. The latter was chosen to improve the decision mainly due to the alcohol sensor limitations previously described. By monitoring the standard deviation of the LRF readings, it is possible to observe that their standard deviation significantly drops when affected by the smoke (Fig. 13). This is an expected behavior since the smoke tends to uniformly constrain the readings. Although we have considered the standard deviation of readings in our experiments, other measures of dispersion or correlation could be used instead.

As Fig. 12 depicts, the overall organization of this architecture resembles the commonly used feedback controllers wherein contextual knowledge is extracted from data, followed by a reasoning phase to provide the adequate information to the robot (*i.e.* map and localization). Hence, based on the alcohol sensor, the sonars and the LRF, one can assess the relation between the inputs and outputs of the fuzzy system. The choice around this relation depends on the characteristics of the readings arising from each source.

Considering the characteristics of the sensors previously highlighted and by observing Fig. 13, one can outline a considerably vague or fuzzy rationale: *"The LRF readings can only be trusted when alcohol readings are below 20 or the standard deviation of the laser readings is above 0.8. If not, only trust the sonar readings whenever it presents readings inferior to 2.5 meters"*.

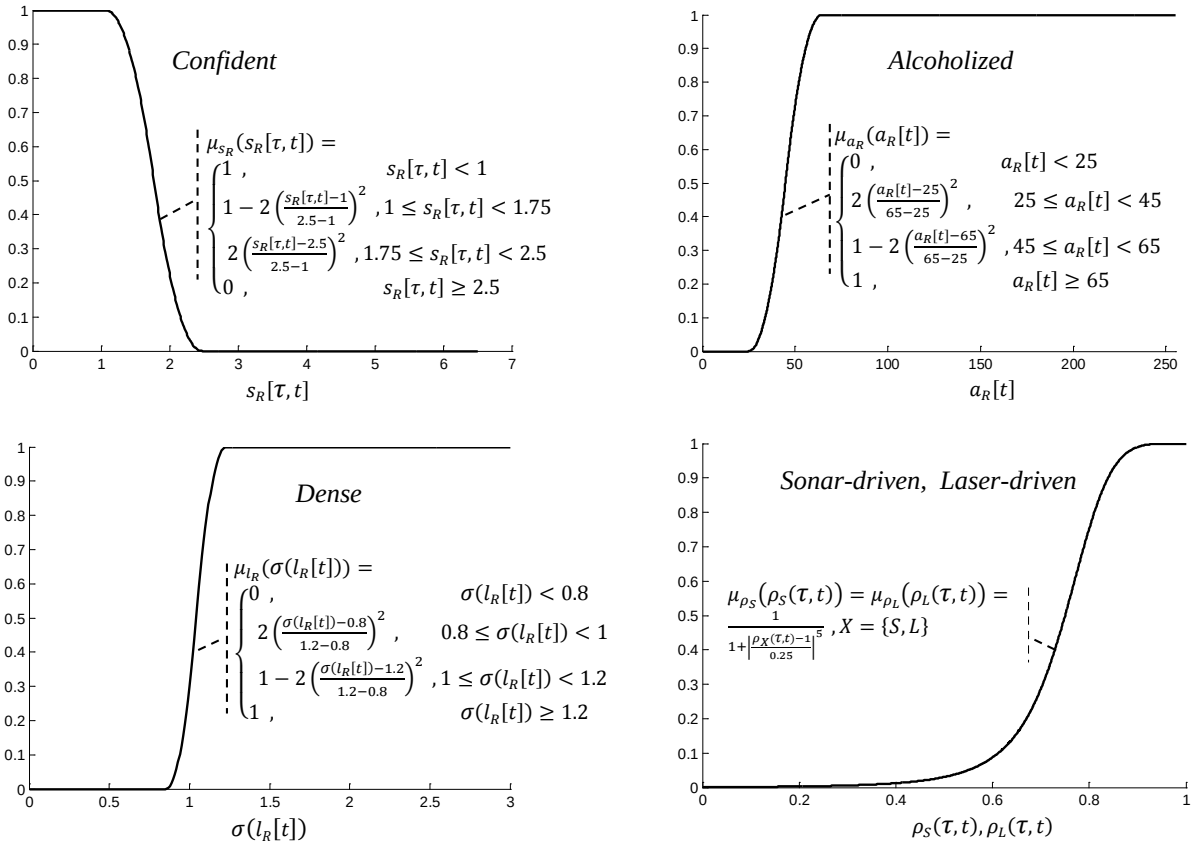

Fig. 14: Membership function for each input and to quantify the consequents: on the top-left, input sonar reading from section τ, $\mu_{s_R}(s_R[\tau,t])$; on the top-right, input alcohol sensor reading, $\mu_{a_R}(a_R[t])$; on the bottom-left, input standard deviation of laser readings, $\mu_{l_R}(\sigma(l_R[t]))$; on the bottom-right, output probabilities $\rho_S(\tau,t)$ and $\rho_L(\tau,t)$.

Although the input information of the system might be imprecise, the results of fuzzy analysis are not. Fuzzy sets need membership functions, *i.e.* mathematical equations that can take certain shapes [31]. Examples of reasonable functions are Π-shaped and bell-shaped functions, because of their simplicity and efficiency when considering computational issues. In spite of this, and considering the above rationale, the membership rules represented in Fig. 14 and described below were defined.

The membership function $\mu_{s_R}(s_R[\tau,t])$ represents how *Confident* the sonar is. The membership function $\mu_{a_R}(a_R[t])$ represents how *Alcoholized* the environment is. The membership function $\mu_{l_R}(\sigma(l_R[t]))$ represents how *Dense* the smoke is.

As for the consequent functions, one can simply define the same bell-shaped membership relation for softening both outputs, as represented in Fig. 14. The *Mamdani-Minimum* [31] was used to quantify the premise and implication. The defuzzification was performed using the center-of-gravity (CoG) method. The CoG is a continuous method and one of the most frequently used in control engineering and process modeling, being represented by the centroid of the composite area of the output fuzzy term.

Considering the above rationale and figures, the following diffuse ***IF-THEN-ELSE*** rules are considered in Algorithm 3.

Algorithm 3: *SmokeNav v2*: Fuzzified Model Pseudocode

1: **if** $a_R[t]$ **is** Alchoholized **or** $\sigma(l_R[t])$ **is** Dense **then**
2: $\quad\rho_L(\tau,t)$ **is** Laser-driven
3: **else if** $S_R[\tau,t]$ **is** Confident **then**
4: $\quad\rho(\tau,t)$ **is** Sonar-driven
5: **end if**

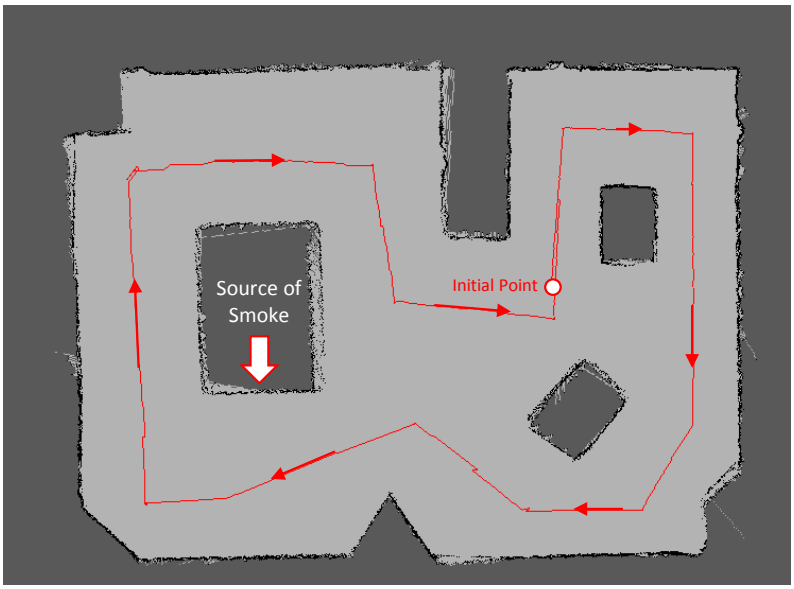

Fig. 15: The modified *R3.2 arena*.

The decision on whether to choose the sonar or the LRF at a given section τ and time t is then evaluated by simply comparing which one has a higher trust probability and if that trust probability is equal or greater than a given threshold. For instance, one will choose the sonar at time t over the LRF readings within the same section if $\rho_S(\tau,t) > \rho_L(\tau,t)$ and $\rho_S(\tau,t) > \rho_T$. In this work, we consider the threshold to be the expected value of an uniform probability distribution with sample space between 0 and 1, *i.e.*, $\rho_T = \frac{1}{2}$.

5.4.1 Results and Discussion

Several experiments with the Scout mobile robot (see Fig. 2b, page 7) in a realistic scenario were performed to validate the *SmokeNav v2* layer using fuzzy logic. A modified test arena was built in the same class room used in the experiments reported in section 5.3.1. Additionally, a run with *GMapping* on the Nomad Scout in this arena with clean conditions was conducted. The resulting map is shown in Fig. 15. In this new version, the Nomad Scout was available, and it was chosen due to the superior performance of the sonar ring when compared to the Pioneer 3-DX, as seen in section 4. As mentioned before, the sonar ring of Scout robot behaves better in most of the situations. For example, in the case of plain corridor, the sonar ring of this robot is able to retrieve more information than the Pioneer's sonar ring.

During these experiments, the same test procedure described in subsection 5.3.1 was considered to evalute the fuzzified approach against one which exclusively uses LRF readings. As before, even when the robot leaves the smoky region, the estimation of the robot's pose using only LRF data becomes erroneous and the SLAM algorithm is not able to correctly recover and update the robot's pose. This is not surprising since the algorithm is only using the LRF readings and the scan matching process fails due to the false readings.

From the analysis of the results shown in Fig. 16, it can be seen that the proposed fuzzy technique allowed to successfully map the arena in most cases. The poor results obtained in the third trial are justified by the higher density of smoke during all the experiment, which was an extreme case. To support the results, the metric used in section 3 to evaluate the performance of different SLAM approaches was used. The resulting error for each trial is shown in Table 4. Also, the usage of sonar data was evaluated by counting the time that sonar data was used along the experiments.

The improvements are significant and it has been shown that SLAM in such harsh conditions is possible using commonly available range sensors in mobile robots and the fuzzified multimodal sensor fusion approach proposed herein. In addition, the developed layer does not introduce significant delays in the system, being adequate for use in real-time. The solution proposed is affordable, using only commercial off-the-shelf (COTS) and fairly cheap sensors. Superior results would be obtained using sonars with more stable readings. Beyond that, it is the authors' belief that a solution based on a radar sensor (instead of sonars) would be more effective, even though much more expensive, to solve the problem while maintaining maps of high quality, regardless the smoke density in the environment.

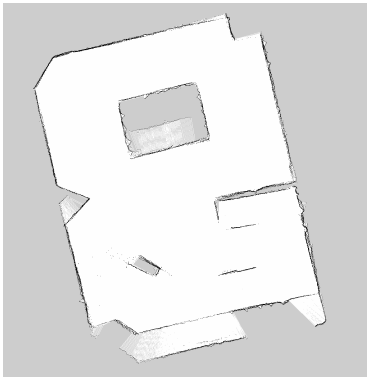

(a) Trial 1: *GMapping* only with LRF data.

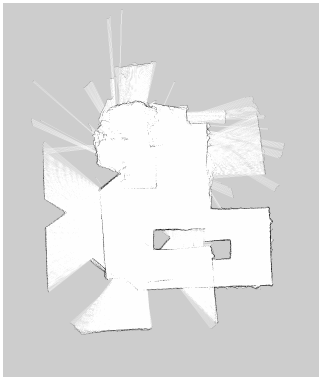

(b) Trial 2: *GMapping* only with LRF data.

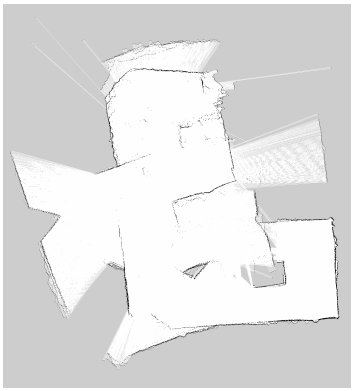

(c) Trial 3: *GMapping* only with LRF data.

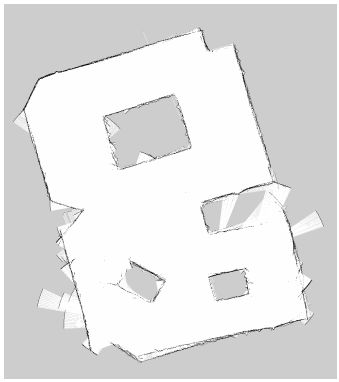

(d) Trial 1: *GMapping* with the *SmokeNav v2* layer.

(e) Trial 2: *GMapping* with the *SmokeNav v2* layer.

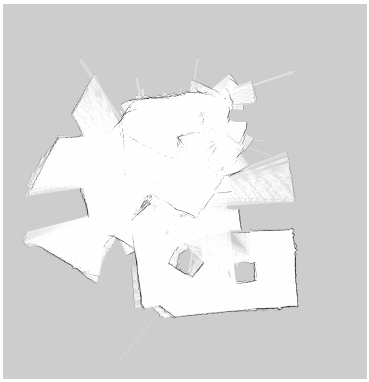

(f) Trial 3: *GMapping* with the *SmokeNav v2* layer.

Fig. 16: Results of three trials. Top images are the resulting maps from *GMapping* only with LRF data and the bottom images are the maps obtained using the *SmokeNav layer v2*.

Table 4: Error estimation for each trial.

Trial	SmokeNav Layer	LRF data	Sonar Usage
1	2.69	18.02	23.33%
2	10.14	19.07	40.25%
3	15.83	23.33	21.53%

6 Conclusion

In this work, a sensor fusion layer for SLAM in low visibility scenarios was proposed. It was verified in the development of the method that the information obtained using only the available two sensory modalities was insufficient in more extreme situations, and we made use of an additional sensor to assess smoke density. A preliminary heuristic version of this technique was presented and the results were discussed. This was fundamental to understand which challenges must be overcome, but also to learn the real impact of the low visibility conditions on mapping tasks. The results obtained are insufficient for a real world application, but mostly because of hardware issues. Despite that, we figured that with the correct choice of ranging sensors it is possible to achieve mapping tasks in adverse conditions.

A second version of sensor fusion layer was proposed in order to overcome the limitations of the preliminary approach. The proposed fuzzified multimodal sensor fusion technique makes use of multiple COTS sensors in order to successfully map environments corrupted by smoke, dust, or steam particles. It is a simple and easily adaptable approach that can be potentially applied with different LRF-based SLAM algorithms, simply by replacing the *GMapping* layer with another algorithm. Experimental results using a Particle Filter 2D SLAM approach proved its functionality. However, hardware limitations still

have and important impact on the results, which are comprehensibly not optimal. Still, it was proved that using the complementary characteristics of multiple range sensors, it is possible to surpass this reduced visibility situation and benefit from the advantages of the distinct range sensors.

Some issues are still left open and correspond to future guidelines that can be followed to improve the current work. Replacing the sonar ring by a range sensor, also immune to smoke but with higher resolution (*e.g.* a UWB radar), would greatly improve the results. The integration of a visual camera to provide a method to detect smoke in the FoV of the LRF, by measuring the gray intensity in the image, could also be explored. Even though the visual camera is highly disturbed by lightning conditions, it can provide richer information about the environment. It would be also interesting to integrate all these changes and validate them through several scenarios with different conditions and more "realistic" smoke. Additionally, an IMU can be integrated in order to increase the accuracy of the localization technique, when sonars and odometry are the only sensors providing valid readings to the robot. At last, and given the modularity of the herein proposed approach, a benchmark of several SLAM methods shall be carried our in order to assess the most fitted combination to be used in scenarios with reduced visibility.

Acknowledgements This work was supported by the CHOPIN research project (PTDC/EEA-CRO/119000/2010) funded by Fundação para a Ciência e a Tecnologia (FCT). In its final stage, the first author was also supported by the EU ICT STRANDS project 600623. The authors would like to thank Prof. Helder Araújo from ISR-Coimbra for providing the Scout mobile robot used in some of the experiments.

References

1. H. Durrant-Whyte and T. Bailey, "Simultaneous Localization and Mapping: Part I," IEEE Robotics and Automation Magazine, vol. 13, no. 2, pp. 99-110 (2006).
2. F. Ferreira, I. Amorim, R. Rocha, and J. Dias, "T-SLAM: Registering Topological and Geometric Maps for Robot Localization in Large Environments," in H. Hahn, H. Ko, and S. Lee (eds.), Multisensor Fusion and Integration for Intelligent Systems, Springer, pp. 423-438 (2009).
3. M. Lazaro, L. Paz, P. Pinies, J. Castellanos, and G. Grisetti, "Multi-Robot SLAM Using Condensed Measurements," in 2013 IEEE/RSJ International Conference on Intelligent Robots and Systems, Tokyo, Japan, pp. 1069-1076 (2013).
4. R. P. Rocha, D. Portugal, M. S. Couceiro, F. Araújo, P. Menezes, and J. Lobo, "The CHOPIN project: Cooperation between Human and rObotic teams in catastroPhic INcidents," in IEEE 13th International Symposium on Safety, Security and Rescue Robotics, Linköping, Sweden (2013).
5. S. Thrun., W. Burgard, D. Fox., "Probabilistic Robotics," MIT Press (2005).
6. S. J. Julier, J.K. Uhlmann, "A counter example to the theory of simultaneous localization and map building," Robotics and Automation, 2001. Proceedings 2001 ICRA. IEEE International Conference on , vol.4, no., pp. 4238-4243, 2001.
7. M. Montemerlo, S. Thrun, D. Koller, B. Wegbreit, "FastSLAM: A Factored Solution to the Simultaneous Localization and Mapping Problem," in AAAI National Conference on Artificial Intelligence, Edmonton, Canada (2002).
8. G. Dissanayake, P. Newman, S. Clark, H. F. Durrant-Whyte, M. Csorba, "A Solution to the Simultaneous Localization and Map Building (SLAM) Problem," in IEEE Transactions on Robotics and Automation, vol. 17, no. 3, pp. 229-241 (2001).
9. S. Huang, G. Dissanayake., "Convergence and Consistency Analysis for Extended Kalman Filter Based SLAM," in IEEE Transactions on Robotics, vol. 23, no. 5, pp. 1036-1049 (2007).
10. G. Grisetti, C. Stachniss, W. Burgard, "Improved Techniques for Grid Mapping With Rao-Blackwellized Particle Filters," in Transactions on Robotics, vol. 23, no. 1, pp. 34-46 (2007).
11. F. Lu, E. Milios, "Globally Consistent Range Scan Alignment for Environment Mapping," in Autonomous Robots, vol. 4, no. 4 , pp. 333-349 (1997).
12. P. Agarwal, G.D. Tipaldi, L. Spinello, C. Stachniss, W. Burgard, "Robust Map Optimization using Dynamic Covariance Scaling," in 2013 IEEE International Conference on Robotics and Automation, Karlsruhe, Germany, pp. 62-69 (2013).
13. S. Kohlbrecher, J. Meyer, O. Von Stryk, U. Klingauf, "A Flexible and Scalable SLAM System with Full 3D Motion Estimation," in 11th IEEE International Symposium on Safety, Security and Rescue Robotics, Kyoto, Japan, (2011).
14. E. Pedrosa, N. Lau, A. Pereira, "Online SLAM Based on a Fast Scan-Matching Algorithm," in L. Correia, L. P. Reis, J. Cascalho (eds.), Progress in Artificial Intelligence, Lecture Notes in Computer Science, vol. 8154, pp. 295-306, Springer (2013).
15. C. Brunner, T. Peynot, and T. Vidal-Calleja, "Automatic Selection of Sensor Modality for Resilient Localisation in Low Visibility Conditions," in 2012 Robotics: Science and Systems, Workshop on Beyond laser and vision: Alternative sensing techniques for robotic perception, Sydney, Australia (2012).
16. T. Deissler and J. Thielecke, "UWB SLAM with Rao-Blackwellized Monte Carlo data association," in International Conference on Indoor Positioning and Indoor Navigation, Zurich, Switzerland, pp. 1-5 (2010).
17. M. Castro and T. Peynot, "Laser-to-radar sensing redundancy for resilient perception in adverse environmental conditions," in Australasian Conference on Robotics and Automation, Sydney, Australia (2012).
18. J. Sales, R. Marín, E. Cervera, S. Rodríguez, and J. Pérez, "Multi-Sensor Person Following in Low-Visibility Scenarios," Sensors, vol. 10, no. 12, pp. 10953-10966 (2010).
19. J. Marti, J. Sales, R. Marín, and P. Sanz, "Multi-Sensor Localization and Navigation for Remote Manipulation in Smoky Areas," in International Journal of Advanced Robotic Systems, vol. 10, no. 211 (2011).
20. J. Pascoal, L. Marques, and A. De Almeida, "Assessment of Laser Range Finders in Risky Environments," in 2008 IEEE/RSJ International Conference on Intelligent Robots and Systems, Nice, France, pp. 3533-3538 (2008).
21. V. Tretyakov and T. Linder, "Range Sensors Evaluation under Smoky Conditions for Robotics Applications," in 11th IEEE International Symposium on Safety, Security, and Rescue Robotics, Kyoto, Japan, pp. 215-220 (2011).

22. F. Pomerleau, A. Breitenmoser, M. Liu, F. Colas, and R. Siegwart, "Noise Characterization of Depth Sensors for Surface Inspections," in 2012 2nd International Conference on Applied Robotics for the Power Industry, Zurich, Switzerland, pp. 16-21 (2012).
23. B. Steux, and O. El Hamzaoui, "tinySLAM: a SLAM Algorithm in Less than 200 Lines C-Language Program," in 2010 11th International Conference on Control Automation Robotics & Vision, Singapore, pp. 1975-1979 (2010).
24. L. Carlone, R. Aragues, J. A. Castellanos, and B. Bona, "A Linear Approximation for Graph-based Simultaneous Localization and Mapping," in Robotics: Science and Systems, Los Angeles, California, USA (2011).
25. R. Vincent, B. Limketkai, and M. Eriksen, "Comparison of Indoor Robot Localization Techniques in the Absence of GPS," in SPIE 7664, Detection and Sensing of Mines, Explosive Objects, and Obscured Targets XV, 76641Z (2010).
26. J. Machado Santos, D. Portugal, and R. P. Rocha, "An Evaluation of 2D SLAM Techniques Available in Robot Operating System," in IEEE 13th International Symposium on Safety, Security and Rescue Robotics, Linköping, Sweden (2013).
27. M. Quigley, K. Conley, B. P. Gerkey, J. Faust, T. Foote, J. Leibs, R. Wheeler, and A. Y. Ng, "ROS: an Open-Source Robot Operating System," in 2009 IEEE International Conference on Robotics and Automation, Workshop on Open Source Software, Kobe, Japan (2009).
28. G. Grisetti, C. Stachniss, and W. Burgard, "Improved Techniques for Grid Mapping With Rao-Blackwellized Particle Filters," IEEE Transactions on Robotics, vol. 23, no. 1, pp. 34-46 (2007).
29. M. S. Couceiro, J. T. Machado, R. P. Rocha, and N. M. Ferreira, "A Fuzzified Systematic Adjustment of the Robotic Darwinian PSO," Robotics and Autonomous Systems, vol. 60, no. 12, pp. 1625-1639 (2012).
30. J. F. Ferreira, and J. Dias, "Probabilistic Approaches to Robotic Perception," Springer Tracts in Advanced Robotics, Vol. 91 (2014).
31. L.A. Zadeh, "Fuzzy Sets, Information and Control," Information and Control, vol. 8, no. 3, pp. 338-353 (1965).